Physics Procedia

Volume 75, 2015, Pages 625–633

20th International Conference on Magnetism

Molecular Spin Dynamics Analysis of Complex Magnetic Structure on the FCC Lattice in Itinerant Electron System

Yoshiro Kakehashi[1], Shota Nohara[1], Sumal Chandra[1], and Takashi Uchida[2]

[1] University of the Ryukyus, Nishihara, Okinawa, Japan
yok@sci.u-ryukyu.ac.jp
[2] Hokkaido University of Science, Teine-Maeda, Sapporo, Japan
uchida@hus.ac.jp

Abstract

The magnetic structure of the Hubbard model on the fcc lattice with competing magnetic interactions has been investigated by means of the Molecular Spin Dynamics (MSD) method. For the Coulomb interaction strength $U/|t| = 8$, the MSD yields the ferromagnetism for electron number n from 2.0 to 1.2, complex ferrimagnetic structures for n from 1.2 to 0.8, complex antiferromagnetic structures between $n = 0.8$ and 0.6, and the paramagnetic state below $n = 0.60$. By making use of the Fourier analysis, it is found that the $3\boldsymbol{Q}$ multiple spin density waves with triple $\boldsymbol{Q}$ wave vectors, the $2\boldsymbol{Q}$ multiple spin density waves with double $\boldsymbol{Q}$ wave vectors, and a complex antiferromagnetic structure with amplitude modulation are realized for $n \approx 0.90$, $n \approx 0.75$, and $n \approx 0.70$, respectively.

Keywords: magnetic structure, molecular spin dynamics, multiple spin density waves, Hubbard model

1 Introduction

Magnetic alloys and related intermetallic compounds often show a variety of magnetic structures due to competition between long-range ferro- and antiferro-magnetic interactions being characteristic of itinerant electrons [1, 2]. In the case of transition metals, the formation of the ferromagnetism in Fe, Co, and Ni is well understood on the basis of the Stoner picture. There the energy gain of Coulomb interactions overcomes the loss of kinetic energy when spins are uniformly polarized. On the other hand, the antiferromagnetic states in γ-Fe, Mn, and Cr with less d electron numbers are characterized by long-range antiferromagnetic interactions. The alloys containing Cr, Mn, and Fe, such as Fe-Cr, Fe-Mn, Ni-Mn, and Mn-Pt alloys, are known to show complex magnetic structures due to the long-range competing interactions [1], which are neither well resolved by experimental techniques nor understood by theoretical investigations.

Theoretical determination of complex magnetic structures is in fact not easy when the interactions are long-range and compete with each other, because many local minima of the free energy are expected in the configuration space of magnetic moments. Because of this

Selection and peer-review under responsibility of the Scientific Programme Committee of ICM 2015

doi:10.1016/j.phpro.2015.12.080

fact, the magnetic phase diagram of itinerant electron system has not been well understood theoretically even for the simple model system.

In this paper we investigate the complex magnetic structure of the single-band Hubbard model on the fcc lattice on the basis of the molecular spin dynamics (MSD) method [2, 3]. The fcc lattice is known to form a network of edge-sharing tetrahedra that leads to a frustration of magnetic moments for the nearest-neighbor antiferromagnetic interactions [4]. We therefore expect a variety of complex magnetic structures due to long-range competing interactions with a change of parameters. The complex magnetic structures are often expressed as a superposition of spin density waves with different wave vectors $\{\boldsymbol{Q}_n\}$, which is called the multiple spin density waves (MSDW). We demonstrate that the MSDW appear between the ferro- and the paramagnetic regions with decreasing electron number.

The MSD method is based on the functional integral method for the spin fluctuation theories [2, 5] and the isothermal molecular dynamics method [6] to the fictitious spin variables. The method allows us to find automatically the magnetic structure and to calculate related magnetic properties of the system at finite temperatures. In the present calculations, we adopt the two-field static approximation to the functional integral technique which reduces to the Hartree-Fock approximation at the ground state, and determine the magnetic structure on the level of the Hartree-Fock approximation, using the MSD at low temperatures.

In the following section, we briefly review the functional integral technique and the MSD method. In Sec. 3, we present numerical results of magnetic structures on the fcc lattice at low temperatures for a given Coulomb interaction strength U. By making use of the Fourier transform of the complex magnetic structures in the real space, we find the single $\boldsymbol{Q}$, the double $\boldsymbol{Q}$, and the triple $\boldsymbol{Q}$ MSDW, varying electron number. In the last section we summarize our results of the MSD calculations, and discuss future problems to be solved.

2 Molecular Spin Dynamics Method

We adopt in this study the single-band Hubbard model on the fcc lattice [7].

$$H = \sum_{i,\sigma} \epsilon_0 \, n_{i\sigma} + \sum_{i,j,\sigma} t_{ij} \, a^{\dagger}_{i\sigma} a_{j\sigma} + U \sum_{i} n_{i\uparrow} n_{i\downarrow} \, . \tag{1}$$

Here $a^{\dagger}_{i\sigma}(a_{i\sigma})$ denotes the creation (annihilation) operator on site i for an electron with spin σ, and $n_{i\sigma} = a^{\dagger}_{i\sigma} a_{i\sigma}$ is the number operator with spin σ on site i. The first term at the r.h.s. (right-hand-side) of Eq. (1) denotes the atomic state with atomic level ϵ_0, the second term denotes electron hopping from site j to site i. t_{ij} is the transfer integral between sites i and j. The last term is the on-site Coulomb interaction term, U being the intra-atomic Coulomb interaction energy parameter.

In the functional integral method, we transform the two-body interactions at the r.h.s. of Eq. (1) into a time-dependent potential with charge and exchange random field variables by making use of the two-field Hubbard-Stratonovich transformation [5]. In the static approximation which neglects the time dependence of field variables, the magnetic moment on site i is given by a semi-classical average of exchange field ξ_i on the same site as follows [8].

$$\langle m_i \rangle = \langle \xi_i \rangle = \frac{\int \Big[\prod_j \sqrt{\frac{\beta U}{4\pi}} d\xi_j \Big] \xi_i \, e^{-\beta E(\xi)}}{\int \Big[\prod_j \sqrt{\frac{\beta U}{4\pi}} d\xi_j \Big] e^{-\beta E(\xi)}} \, . \tag{2}$$

Here β denotes the inverse temperature, $E(\xi)$ is an effective potential defined by

$$E(\xi) = \int d\omega f(\omega) \frac{1}{\pi} \mathrm{Im}\,\mathrm{Tr}\big[\ln(z - \boldsymbol{H}(\xi))\big] + \sum_i \frac{1}{4} U \left(\xi_i^2 - \zeta_i^2(\xi)\right). \tag{3}$$

Here $z = \omega + i\delta$, δ being an infinitesimal positive number. $f(\omega)$ is the Fermi distribution function, $\boldsymbol{H}(\xi)$ is a one-electron Hamiltonian matrix defined by

$$(\boldsymbol{H}(\xi))_{ij\sigma} = \left(\epsilon_0 - \mu + \frac{1}{2} U \zeta_i(\xi) - \frac{1}{2} U_i \xi_i \sigma\right) \delta_{ij} + t_{ij}(1 - \delta_{ij}) \ , \tag{4}$$

and μ is the chemical potential. $\zeta_i(\xi)$ denotes the local charge on site i when the exchange fields $\{\xi_j\}$ are given. The second term at the r.h.s. of Eq. (3) expresses the Gaussian quadratic terms for random exchange and charge fields.

Note that one can take the saddle point $\{\xi_i^*\}$ in Eq. (2) at the ground state; $\partial E(\xi^*)/\partial \xi_i = 0$. This condition leads to the Hartree-Fock equation, $\xi_i^* = \langle m_i \rangle_0$. Here the average $\langle \sim \rangle_0$ is taken with respect to the Hartree-Fock Hamiltonian $\boldsymbol{H}(\xi^*)$.

We calculate here the thermal average of spin, *i.e.*, Eq. (2) with use of the isothermal molecular dynamics (MD) method [6]; we assume the ergodicity of the system with a potential $E(\xi)$, and calculate the average (2) by means of the time average of variable $\xi_i(t)$.

$$\langle m_i \rangle = \lim_{t_0 \to \infty} \frac{1}{t_0} \int_0^{t_0} \xi_i(t) dt \ . \tag{5}$$

The dynamics of $\{\xi_i(t)\}$ which produces the ensemble average (2) is given by

$$\dot{\xi}_i = \frac{1}{\mu_{\mathrm{LM}}} p_i \ , \tag{6}$$

$$\dot{p}_i = \frac{1}{2} U (\langle m_i \rangle_0 - \xi_i) - \eta \, p_i \ , \tag{7}$$

$$\dot{\eta} = \frac{1}{K} \left(\sum_i \frac{p_i^2}{\mu_{\mathrm{LM}}} - NkT \right) \ . \tag{8}$$

Here μ_{LM} is an effective mass for a fictitious local moment $\xi_i(t)$ on site i, p_i is the momentum being conjugate to $\xi_i(t)$. The first term at the r.h.s. of Eq. (7) denotes a magnetic force defined by $-\partial E(\xi)/\partial \xi_i$, and the second term is the friction force describing heat-bath effects. The time-dependent friction coefficients $\eta(t)$ is determined by Eq. (8) to keep temperature T constant. K and k are a constant parameter and the Boltzmann constant, respectively. N denotes the number of atoms of the system. The local magnetic moment $\langle m_i \rangle_0$ at each time step is calculated by means of the recursion method [9]. The terminator in the recursion method is calculated self-consistently with use of the effective medium technique [3].

The MSD method is much faster than the usual method in finding the most stable magnetic structure. In fact, in a simple method of the Hartree-Fock approximation, we need the data points of 10^N, assuming 10 mesh points for each local variable ξ_i, in order to sweep all the possible configurations of magnetic moments. In the MSD method, we only need $10^4 \times N$ MD data points for 10^4 MD time steps to obtain the most stable magnetic structure. In the actual MSD simulation, we consider a large MD unit cell. The latter is further surrounded by 27 MD unit cells with effective medium.

3 Numerical Results

In the numerical calculations, we adopted the Hubbard model with nearest-neighbor transfer integral t on the fcc lattice and the MD unit cell consisting of $8 \times 8 \times 8$ fcc unit cells. The Coulomb interaction strength is fixed to be $U/W = 0.5$, where $W = 16|t|$ is the band width of the system. We performed the MSD calculations for various electron numbers per atom n at constant temperature $T/|t| = 0.001$, which is one-hundredth of typical Curie temperature around $n = 1.5$. The magnetic structures were calculated by averaging the local moments over the last $3000 \sim 4000$ MD steps.

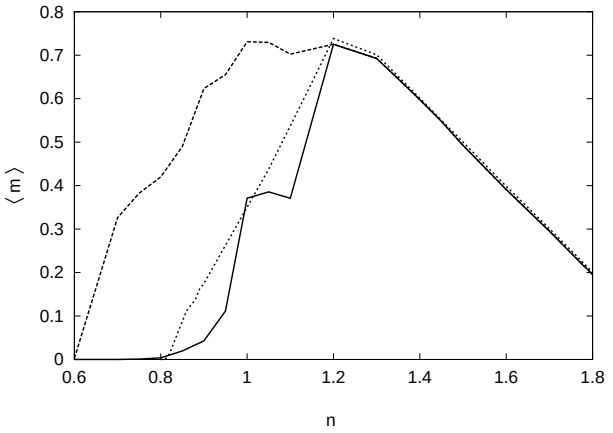

Figure 1: Magnetic moments as a function of electron number (n). Solid curve:magnetization per atom $\langle m \rangle$, dotted curve : magnetization obtained from the Hartree-Fock ferromagnetic solution at the ground state, dashed curve: average amplitude $(\sum_i \langle m_i \rangle^2/N)^{1/2}$.

Figure 1 shows the average magnetic moments as a function of electron number n. From $n = 2.0$ to 1.3, the system shows a strong ferromagnetism, where the magnetization linearly increases with decreasing n. Below $n = 1.3$, the magnetization deviates from the linear curve, indicating the appearance of holes in the up spin band, and rapidly decreases from $n = 1.2$ with decreasing n. It vanishes at $n = 0.8$. The average amplitude defined by $(\sum_i \langle m_i \rangle^2/N)^{1/2}$, on the other hand, deviates from the magnetization curve below $n = 1.2$, shows a broad peak around $n = 1.0$, and remains finite up to $n = 0.6$. We therefore expect various magnetic structures between $n = 0.6$ and $n = 1.2$.

We present the real space magnetic structure for $n = 1.1$ in Fig. 2. Although there are up and down magnetic moments, the magnetic structure seems to be complex. We therefore performed the Fourier analysis using the following relation.

$$\langle m_i \rangle = \sum_{\boldsymbol{Q}}^{\mathrm{BZ}} m(\boldsymbol{Q}) e^{i\boldsymbol{Q}\cdot\boldsymbol{R}_i} \ . \tag{9}$$

Here $\boldsymbol{Q} = \Big(n_1/N_x, n_2/N_y, n_3/N_z\Big)2\pi/a$, and N_x, N_y, N_z denote size of a MD unit cell in unit of a lattice constant a. $\boldsymbol{R}_i$ denotes the position vector of site i. The Fourier components are

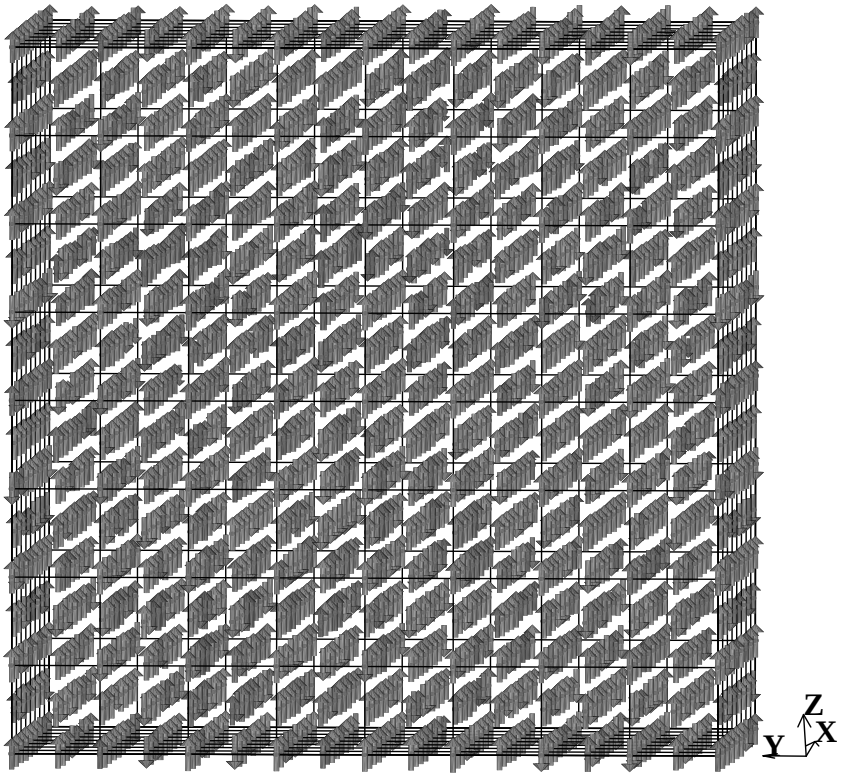

Figure 2: Calculated magnetic structure on the $8 \times 8 \times 8$ fcc lattice for $n = 1.10$.

calculated from the inverse relation,

$$m(\boldsymbol{Q}) = \frac{1}{N_c} \sum_{i}^{N_c} \langle m_i \rangle e^{-i\boldsymbol{Q}\cdot\boldsymbol{R}_i} \ , \tag{10}$$

$N_c\,(= 2048)$ being the number of atoms in a MD unit cell. Figure 3 shows the distribution of the Fourier amplitudes ($|m(\boldsymbol{Q})|^2$) in the Brillouin zone (BZ). We find various $\boldsymbol{Q}$ components in addition to a large ferromagnetic component at $\boldsymbol{Q} = \boldsymbol{0}$.

When $n = 0.90$, the magnetization almost vanishes and alternative change of magnetic moment appears as shown in Fig. 4. The result of the Fourier analysis is shown in Fig. 5. The $\boldsymbol{Q} = \boldsymbol{0}$ ferromagnetic component is negligible. Instead, we find the magnetic structure characterized by $3\boldsymbol{Q}$ components: $\hat{\boldsymbol{Q}}_1 = (1,0,0)2\pi/a$, $\hat{\boldsymbol{Q}}_2 = (0,1,0)2\pi/a$, $\hat{\boldsymbol{Q}}_3 = (0,0,1)2\pi/a$. It is described approximately as

$$\begin{aligned} \langle m_i \rangle \ &= \ 2|m(\hat{\boldsymbol{Q}}_1)| \cos(\hat{\boldsymbol{Q}}_1 \cdot \boldsymbol{R}_i) \\ &\quad +2|m(\hat{\boldsymbol{Q}}_2)| \cos(\hat{\boldsymbol{Q}}_2 \cdot \boldsymbol{R}_i - \pi) + 2|m(\hat{\boldsymbol{Q}}_3)| \cos(\hat{\boldsymbol{Q}}_3 \cdot \boldsymbol{R}_i) \ , \end{aligned} \tag{11}$$

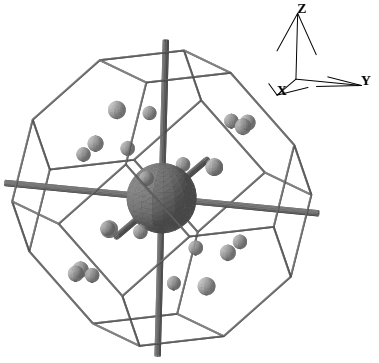

Figure 3: Distribution of the Fourier amplitudes $|m(\boldsymbol{q})|^2$ in the first Brillouin zone for $n = 1.10$. The volume of each sphere is drawn to be proportional to the amplitude $|m(\boldsymbol{q})|^2$.

with $|m(\hat{\boldsymbol{Q}}_1)| = 0.126$, $|m(\hat{\boldsymbol{Q}}_2)| = 0.072$, and $|m(\hat{\boldsymbol{Q}}_3)| = 0.151$. This is a $3\boldsymbol{Q}$ multiple spin density waves (MSDW).

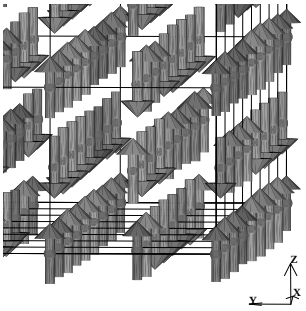

Figure 4: Calculated magnetic structure for $n = 0.90$ (enlarged).

When the electron number is decreased, the second amplitude $|m(\hat{\boldsymbol{Q}}_2)|^2$ becomes smaller. We present the amplitude distribution for $n = 0.75$ in Fig. 6. In this case, the magnetic moment $\langle m_i \rangle$ is basically approximated by $2\boldsymbol{Q}$ components:

$$\langle m_i \rangle \quad = \quad 2|m(\hat{\boldsymbol{Q}}_1)| \cos(\hat{\boldsymbol{Q}}_1 \cdot \boldsymbol{R}_i) + 2|m(\hat{\boldsymbol{Q}}_3)| \cos(\hat{\boldsymbol{Q}}_3 \cdot \boldsymbol{R}_i - \pi) \ , \tag{12}$$

with $|m(\hat{\boldsymbol{Q}}_1)| = 0.079$, and $|m(\hat{\boldsymbol{Q}}_3)| = 0.034$. This is a $2\boldsymbol{Q}$ MSDW.

When electron number is decreased further, the $\hat{\boldsymbol{Q}}_3$ component becomes weaker in amplitude. We present the amplitude distribution for $n = 0.70$ in Fig. 7. The magnetic moment is approximately given by a single $\hat{\boldsymbol{Q}}_1 = (1, 0, 0)2\pi/a$ as follows.

$$\langle m_i \rangle \quad = \quad 2|m(\hat{\boldsymbol{Q}}_1)| \cos(\hat{\boldsymbol{Q}}_1 \cdot \boldsymbol{R}_i - \pi) \ , \tag{13}$$

with $|m(\hat{\boldsymbol{Q}}_1)| = 0.099$. This is the antiferromagnetic structure of the first kind. However, it should be noted that the actual $\boldsymbol{Q}$ points deviate from $\hat{\boldsymbol{Q}}_1$ by $\boldsymbol{q} = (0, \pm 1/8, 0)2\pi/a$, so that the amplitude $|m(\hat{\boldsymbol{Q}}_1)|$ is modulated by a factor $\cos(\boldsymbol{q} \cdot \boldsymbol{R}_i)$ with a period $8a$.

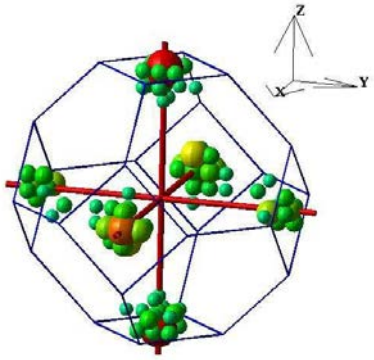

Figure 5: Distribution of the Fourier amplitudes $|m(\boldsymbol{q})|^2$ in the first Brillouin zone for $n = 0.90$.

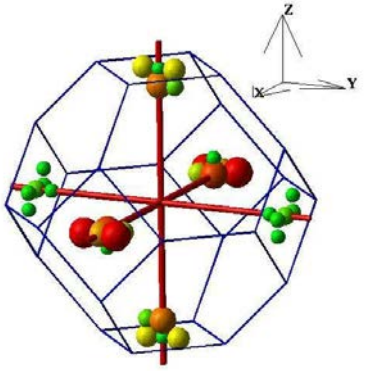

Figure 6: Distribution of the Fourier amplitudes $|m(\boldsymbol{q})|^2$ for $n = 0.75$.

In conclusion, the magnetic phase diagram for $U/W = 1/2$ obtained in the MSD analyses is summarized as follows. For $n > 1.3$, a strong ferromagnetism with uniform polarization is realized. Between $n = 1.2$ and 1.3, a weak ferromagnetism with holes in up spin band appears. With decreasing electron number, the magnetization rapidly decreases with reverse of local magnetic moments, and the ferrimagnetic state is realized. Around $n = 0.90$ we find a $3\boldsymbol{Q}$ MSDW with the wave vectors $\hat{\boldsymbol{Q}}_1 = (1, 0, 0)2\pi/a$, $\hat{\boldsymbol{Q}}_2 = (0, 1, 0)2\pi/a$, $\hat{\boldsymbol{Q}}_3 = (0, 0, 1)2\pi/a$, a $2\boldsymbol{Q}$ MSDW with $\hat{\boldsymbol{Q}}_1$ and $\hat{\boldsymbol{Q}}_3$ around $n = 0.75$, and the first-kind antiferromagnetic structure with amplitude modulation around $n = 0.70$. Finally, the nonmagnetic state is realized below $n = 0.60$.

4 Summary

We have investigated the complex magnetic structures of the Hubbard model on the fcc lattice by making use of the molecular spin dynamics (MSD) method which allows us to find automatically magnetic structures of the system on the level of the Hartree-Fock mean-field

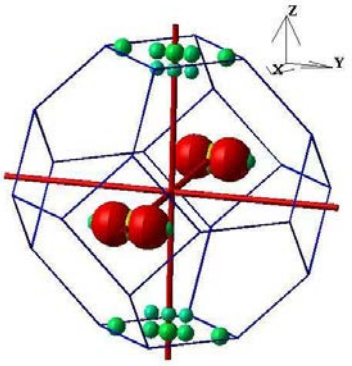

Figure 7: Distribution of the Fourier amplitudes $|m(\boldsymbol{q})|^2$ for $n = 0.70$.

approximation. We obtained the magnetic structure for the nearest-neighbor transfer integral t and the Coulomb interaction strength $U/|t| = 8$. The simple ferromagnetism appears in the range $1.2 < n < 2.0$. In the range $0.80 < n < 1.2$, we found complex ferrimagnetism with local magnetic moments antiparallel to the magnetization. In particular, the $3\boldsymbol{Q}$ MSDW appears around $n = 0.90$. Below $n = 0.80$, we found complex antiferromagnetic structures, *i.e.*, $2\boldsymbol{Q}$ MSDW around $n = 0.75$ and $1\boldsymbol{Q}$ SDW with amplitude modulation around $n = 0.70$.

The magnetic structures obtained by decreasing electron number seem to be closely related to some of those in transition metals and alloys, though our model Hamiltonian is too simple to describe the real systems. The strong ferromagnetism and rapid collapse of the ferromagnetism in the range of $0.8 < n < 2.0$ is found in Fe_xNi_{1-x} $(0.0 < x < 0.7)$ and Fe_xCo_{1-x} $(0.0 < x < 0.8)$ alloys. The $3\boldsymbol{Q}$ MSDW found for $n \approx 0.9$ is suggested to be realized in γ-Fe_xMn_{1-x} $(0.4 < x < 0.7)$ and $Ni_{28}Mn_{72}$ alloys, though they are non-collinear [1]. The $1\boldsymbol{Q}$ SDW with $\hat{\boldsymbol{Q}}_3 = (0, 0, 1)2\pi/a$ (*i.e.*, the antiferromagnetic structure with the first kind) is found in γ-Mn and γ-Fe_xMn_{1-x} $(0.7 < x < 0.9)$ alloys. The $1\boldsymbol{Q}$ SDW with amplitude fluctuations found near the boundary between the para- and antiferro-magnetic states may correspond to the SDW's in Cr-V alloys with $\boldsymbol{Q} \approx (0, 0, 0.95)2\pi/a$, though these alloys are based on the bcc lattice. We have to perform further the MSD calculations changing the Coulomb interaction strength U in order to complete the magnetic phase diagram on the $U-n$ plane.

Present calculations are limited to the collinear case of magnetic structure because we adopted the two-field static approximation to the functional integral method. When we allow the non-collinear magnetic structure, we expect that the ferro- and ferri-magnetic region are reduced because of a possible rotation of magnetic moments in the region $1.0 \lesssim n \lesssim 1.3$. In this case, the noncollinear $3\boldsymbol{Q}$ MSDW are more favorable according to the phenomenological theory of magnetic structure [10].

It is possible to perform the non-collinear calculations. In this case, we first introduce the locally-rotated coordinates at each site and adopt the two-field static approximation to the functional integral method. After taking average over polar angles at each site, we obtain the effective potential for non-collinear calculations. The MSD calculations with non-collinearity are in progress.

Acknowledgement

This work was supported by Grant-in-Aid for Scientific Research (25400404). Numerical calculations have been partly carried out with use of the SGI ICE-XA/UV Hybrid System in the Supercomputer Center, Institute of Solid State Physics, University of Tokyo.

References

[1] H.P.J. Wijn, *Magnetic Properties of Metals* (Springer-Verlag, Heidelberg, 1991).

[2] Y. Kakehashi, *Modern Theory of Magnetism in Metals and Alloys* (Springer-Verlag, Heidelberg, 2012).

[3] Y. Kakehashi, S. Akbar, and N. Kimura, Phys. Rev. **57**, 8354 (1998).

[4] C. Lacroix, P. Mendels, and F. Mila, *Introduction to Frustrated Magnetism* (Springer-Verlag, Heidelberg, 2011).

[5] G. Morandi, E. Galleani, D'Agliano, F. Napoli, C.F. Ratto, Adv. Phys. **23**, 867 (1974).

[6] S. Nosé, J. Chem. Phys. **81**, 511 (1984).

[7] J. Hubbard, Proc. R. Soc. London, Ser. A **276**, 238 (1963); Ser. A **281**, 401 (1964).

[8] Y. Kakehashi and P. Fulde, Phys. Rev. B **32**, 1595 (1985).

[9] R. Haydock, V. Heine, and M.J. Kelly, J. Phys. C **8**, 591 (1975).

[10] T. Uchida and Y. Kakehashi, J. Phys. Soc. Jpn. **75**, 094703 (2006); *ibid.* **76**, 087001 (2007).